Nanoscale Horizons

ROYAL SOCIETY OF CHEMISTRY

COMMUNICATION

View Article Online
View Journal | View Issue

Cite this: *Nanoscale Horiz.*, 2025, **10**, 2908

Received 19th April 2025,
Accepted 6th August 2025

DOI: 10.1039/d5nh00257e

rsc.li/nanoscale-horizons

Ultrathin DNA–copper nanosheets with antibacterial and anti-biofilm activity for treatment of infected wounds

Fangfang Chen,[a] Mengyan Lei,[a] Jing Luo,[b] Jiaqi Li,[b] Jinfang Wang,[a] Nan Zhang,[b] Xinyi Li,[a] Nan Jia,[b] Xiangyuan Ouyang *[ac] and Huaiyu Bu*[b]

The development of innovative antibacterial materials is crucial for addressing wounds infected with bacterial biofilms. Advanced nanomaterials that enable non-antibiotic antibacterial strategies offer new possibilities for treating bacterial infections by eliminating pathogens without relying on antibiotics. Herein, we introduce non-toxic and biocompatible DNA–copper cluster nanosheets (DNS/CuNCs) as effective antibacterial agents. DNS/CuNCs can reduce bacterial surface motility and the secretion of virulence factors by interfering with quorum sensing, and thereby inhibit biofilm formation and enhance their potential as prophylactic antibacterial agents. Notably, DNS/CuNCs exhibit significant *in vitro* bactericidal activity against *Staphylococcus aureus* and *Pseudomonas aeruginosa* and disrupt established surface biofilms in the presence of hydrogen peroxide (H_2O_2). This is attributed to the synergistic effects of their physical ultrathin properties and peroxidase-like activity, which lead to an increase in intracellular ROS levels in bacteria, thereby achieving antibacterial and biofilm-disrupting effects. *In vivo*, DNS/CuNCs effectively eradicate bacterial infections, promote wound healing, and restore normal tissue morphology without toxicity to mammalian cells. With their combined abilities to inhibit biofilm formation, exhibit antibacterial activity, and disrupt biofilms, along with excellent biocompatibility, DNA-templated CuNCs emerge as highly promising candidates for preventive and clinical antibacterial therapies.

New concepts

We employed a green and straightforward approach to synthesize CuNCs using DNA nanosheets (DNS) as templates. The addressability and programmability of DNA nanosheets make them an ideal scaffold for the controlled synthesis of CuNCs, allowing for precise control over their nucleation sites and thickness. These DNS-templated CuNCs (DNS/CuNCs) exhibited the capacity to inhibit biofilm formation, broad-spectrum antibacterial activity *in vitro*, and the ability to disrupt mature biofilms. The results demonstrated that DNS/CuNCs inhibited biofilm formation by disrupting bacterial quorum sensing (QS) mechanisms. Moreover, the synergistic effects of the physical ultrathin properties and peroxidase-like activity of DNS/CuNCs result in elevated intracellular ROS levels in bacteria, thereby effectively killing the bacteria and disrupting biofilms. The *in vivo* antibacterial performance of DNS/CuNCs was evaluated using a mouse skin infection model induced by *Staphylococcus aureus*. To our knowledge, this study is the first to demonstrate that DNA-based nanomaterials can serve as a non-antibiotic strategy for antibacterial agents, capable of inhibiting biofilm formation, killing bacteria, and disrupting mature biofilms. Owing to their safety and excellent biocompatibility, DNS/CuNCs present significant potential for applications in preventive and clinical anti-infection therapies.

Introduction

Bacterial infections represent a critical global health challenge, causing millions of illnesses and deaths annually.[1] The extensive use of antibiotics has led to the emergence of drug-resistant strains that secrete extracellular polymeric substances (EPS), forming biofilms that serve as a protective barrier against antibiotics.[2] Biofilms are particularly problematic, as they can be up to 1000 times more resistant to antibiotics than their planktonic counterparts, making them a major cause of persistent and recurrent infections.[3] Treating resistant strains often requires higher antibiotic doses, which can cause severe side effects such as immune dysfunction, kidney damage, and gastrointestinal issues, while also accelerating the emergence of new resistance mechanisms.[4,5] Given the rapid rise of antibiotic resistance, there is an urgent need for non-antibiotic strategies to combat bacterial and bacterial biofilm-associated infections.

[a] *Key Laboratory of Functional Supramolecular Structure and Materials, Key Laboratory of Synthetic and Natural Functional Molecule of Ministry of Education, College of Chemistry and Materials Science, Northwest University, Xi'an, Shaanxi, 710127, P. R. China. E-mail: ouyangxy@nwu.edu.cn*

[b] *Key Laboratory of Resource Biology and Biotechnology in Western China, Ministry of Education, Provincial Key Laboratory of Biotechnology, College of Life Sciences, Northwest University, Xi'an, Shaanxi, 710069, P. R. China. E-mail: buhy@nwu.edu.cn*

[c] *State Key Laboratory of Chemo/Biosensing and Chemometrics, Hunan University, Changsha, Hunan, 410082, P. R. China*

The rapid advancement of nanotechnology offers promising approaches to combat resistant bacteria.[6] Recently, nanomaterials, including metal/metal oxide,[7,8] carbon-based,[9] liposomal,[10] and polymer-based varieties,[11] have demonstrated significant antibacterial properties for treating drug-resistant bacterial infections. Particularly, metal-based nanomaterials have garnered considerable attention due to their advantageous physicochemical properties, which contribute to their potent antibacterial activity.[12] However, the inherent cytotoxicity and environmental concerns associated with certain metal nanoparticles, such as Ag,[13] prompt the search for safer, more biocompatible alternatives.

DNA is generally regarded as safe, biocompatible, and minimally toxic. Consequently, DNA nanomaterials have garnered significant research interest in the fields of antibacterial applications and biofilm studies due to their unique biocompatibility, programmability, and multifunctionality. Wu *et al.* studied a DNA nanobiocide that loads abundant DNA enzymes (G4/heme) and the broad-spectrum antibiotic levofloxacin (LEV) onto a DNA origami framework. This configuration harnesses reactive oxygen species produced by ribozyme catalysis to disrupt bacterial membrane structures, thereby promoting the rapid penetration of antibiotics into the bacteria and achieving effective bactericidal effects.[14] Xu *et al.* used tobramycin (Tob) as a medium for assembling DNA nanostructures, achieving functionalization through the combination of DNA and antibiotics. The maleimide-modified Tob/DNA nanotubes (NTTob-Mal) constructed in this study exhibited the capability to inhibit biofilm formation of *Pseudomonas aeruginosa* (PA) *in vitro*.[15] However, to date, there have been no reports on non-antibiotic strategies that employ DNA nanostructures for simultaneous antibacterial and biofilm disruption applications. In this study, we employed a green and straightforward approach to synthesize CuNCs using DNA nanosheets (DNS) as templates. The addressability and programmability of DNA nanosheets make them an ideal scaffold for the controlled synthesis of CuNCs, allowing for precise control over their nucleation sites and thickness. These DNS-templated CuNCs (DNS/CuNCs) exhibited the capacity to inhibit biofilm formation and broad-spectrum antibacterial activity *in vitro*, and the ability to disrupt mature biofilms. The results demonstrated that DNS/CuNCs inhibited biofilm formation by disrupting bacterial quorum sensing (QS) mechanisms. Moreover, the synergistic effects of the physical ultrathin properties and peroxidase-like activity of DNS/CuNCs result in elevated intracellular ROS levels in bacteria, thereby effectively killing the bacteria and disrupting biofilms. The *in vivo* antibacterial performance of DNS/CuNCs was evaluated using a mouse skin infection model induced by *Staphylococcus aureus*. To our knowledge, this study is the first to demonstrate that DNA-based nanomaterials can serve as a non-antibiotic strategy for antibacterial agents, capable of inhibiting biofilm formation, killing bacteria, and disrupting mature biofilms. Owing to their safety and excellent biocompatibility, DNS/CuNCs present significant potential for application in preventive and clinical anti-infection therapies.

Results and discussion

Preparation of DNS/CuNCs

An illustration of the self-assembly process of DNS/CuNCs is shown in Fig. 1A and B. The DNS framework was designed based on our previous work to synthesize DNS/CuNCs.[16,17] The DNS framework had two repeating units tile A and tile B (Fig. S1) (sequence shown in Table S1). Both tiles contained two crucial domains: Domain 1 was applied to self-assembly by hybridizing the two repeating DNA tiles through sticky ends, thereby promoting extensive two-dimensional growth in both longitudinal and lateral orientations. Domain 2 was composed of sequences (highlighted in green in Fig. 1A) that acted as metal-binding sites for Cu^{2+} ions. These sites served as controllable nucleation points for CuNCs due to the addressability and programmability of the DNA nanostructure, enabling precise control over density and spacing during CuNC growth. To synthesize DNS/CuNCs, the prepared DNS was incubated with $CuSO_4$ in a buffer solution containing MOPS (20 mM, pH 7.5) and NaCl (150 mM) for 5 minutes. Sodium ascorbate (SA) was then added to the mixture. The Cu^{2+} ions were adsorbed onto the designated sites of the DNS framework and subsequently reduced to form Cu clusters by SA. This reduction process, confined within the two-dimensional structure of DNS, resulted in the formation of DNS/CuNCs nanosheets within 10 minutes at room temperature. Atomic force microscopy (AFM) was employed to confirm the formation of DNS/CuNCs nanosheets. As shown in Fig. 1C and E, the height of DNS was approximately 1.26 nm and the width was 400 nm, demonstrating the successful synthesis of the sheet-like structure DNS. From Fig. 1D and E, the average height and width of DNS/CuNCs had increased to 1.82 ± 0.2 nm and 0.846 ± 0.2 μm ($N = 100$) (Fig. S2), indicating the successful assembly of DNS/CuNCs nanosheets. The height corresponded to the thickness of six to nine layers of copper atoms, given that the diameter of a single copper atom is 255.6 pm.[16] Transmission electron microscopy (TEM) images (Fig. 1F and Fig. S3) further demonstrated the successful synthesis of DNS/CuNCs nanosheets, with a length exceeding 36 μm and a width ranging from 1.5 to 3 μm. This further illustrated that DNS/CuNCs had large lateral dimensions and ultra-thin characteristics. Energy-dispersive X-ray (EDX) spectroscopy analysis confirmed the presence of elements involved in the synthesis of DNS/CuNCs (Fig. 1G). The composition analysis revealed high amounts of Cu, P, and O, with a homogeneous distribution of Cu in the DNS/CuNCs, reflecting the uniformity of nucleation sites with controllable density and spacing. X-ray photoelectron spectroscopy (XPS) was conducted on the DNS/CuNCs samples to further characterize the material. Peaks corresponding to C, N, O, S, P, and Cu were clearly observed (Fig. S4). Notably, two pronounced peaks at 932.8 eV and 952.7 eV were attributed to the binding energies of Cu(0) in the Cu $2p_{3/2}$ and Cu $2p_{1/2}$ states, respectively (Fig. 1H), consistent with previously reported DNA-templated Cu nanoclusters in the literature.[16]

Antibacterial activity of DNS/CuNCs *in vitro*

Gram-positive (*Staphylococcus aureus*, *S. aureus*) and Gram-negative (*Pseudomonas aeruginosa*, *P. aeruginosa*) bacteria were

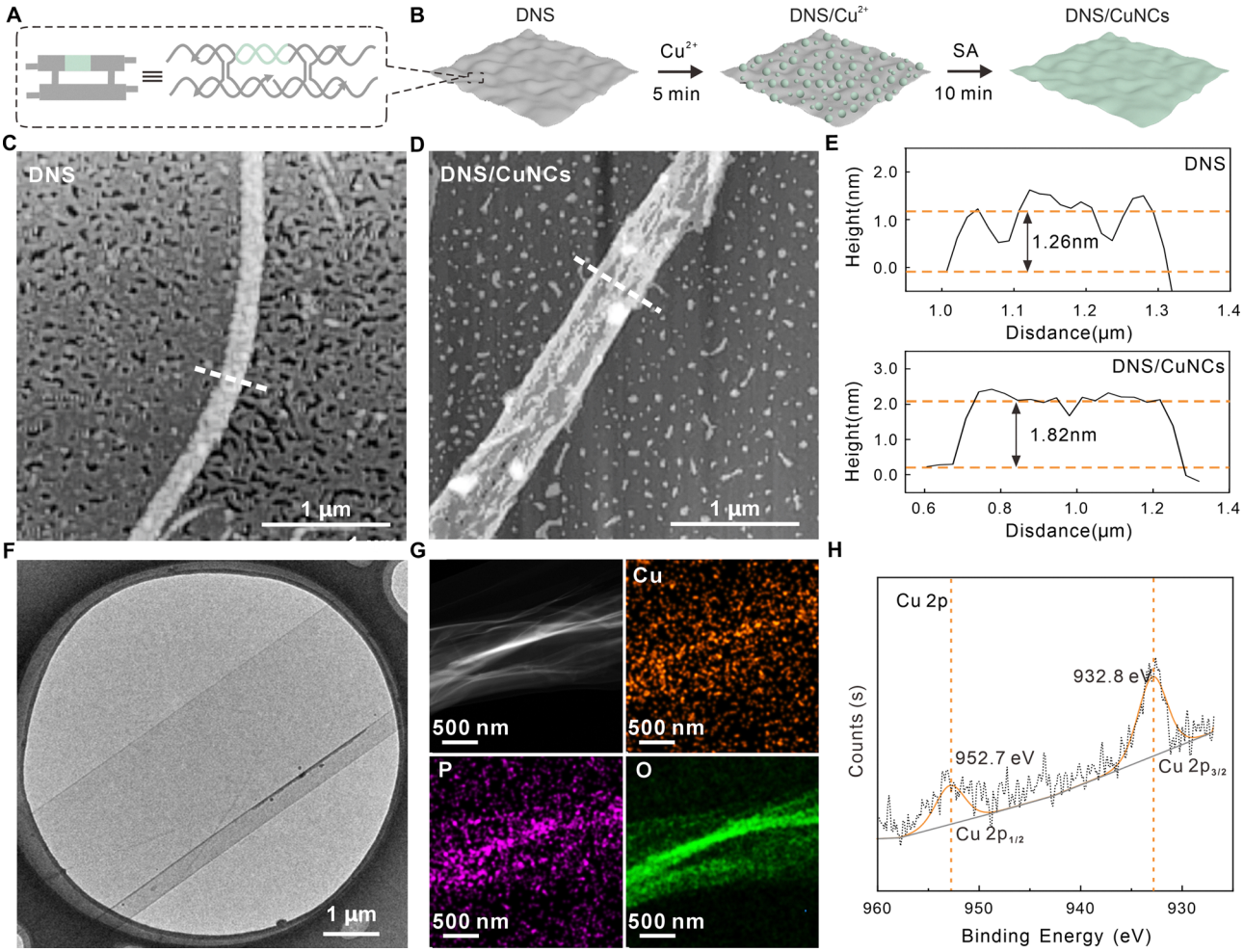

Fig. 1 Preparation and characterization of DNS/CuNCs. (A) and (B) Schematic diagram of the design synthesis of DNS/CuNCs. (C) AFM images of DNS. (D) AFM images of DNS/CuNCs. (E) The AFM height profiles along the white dashed lines in (C) DNS and (D) DNS/CuNCs. (F) TEM images of DNS/CuNCs. (G) High-angle annular dark-field (HAADF) image and energy-dispersive X-ray spectroscopy (EDX) elemental mappings of DNS@CuNCs. (H) X-ray photoelectron spectroscopy (XPS) spectrum of DNS@CuNCs (Cu $2p_{1/2}$ and Cu $2p_{3/2}$ core peaks).

selected as model bacteria to investigate the antibacterial activity of DNS/CuNCs. We introduced copper nanoparticles (CuNPs) and dsDNA-templated copper nanoclusters (dsDNA/CuNCs) as control groups to compare their antibacterial activities with those of DNS/CuNCs. The CuNPs were synthesized without a DNA template, but otherwise, the synthetic procedure was the same as that for DNS/CuNCs. TEM imaging revealed that individual CuNPs were highly monodisperse with an average diameter of 4.8 ± 1.2 nm (based on TEM statistical data, $N = 100$) (Fig. S5). In contrast to the CuNPs, DNS/CuNCs showed significantly higher efficacy in inhibiting *S. aureus* and *P. aeruginosa* (Fig. S6). The same procedure was followed in the synthesis of dsDNA/CuNCs as in that of DNS/CuNCs, utilizing a dsDNA template. AFM imaging of the synthesized dsDNA/CuNCs demonstrated a highly monodisperse morphology with a smaller average diameter of 1.5 ± 0.4 nm (based on AFM statistical data, $N = 100$) (Fig. S7). The antibacterial activities of dsDNA/CuNCs and DNS/CuNCs were evaluated by constructing growth curves through the measurement of the optical density (OD) at 600 nm. As shown in Fig. S8, compared to the PBS group and the corresponding DNA template control group, dsDNA/CuNCs and DNS/CuNCs showed relatively higher inhibitory effects. Furthermore, DNS/CuNCs demonstrated a relatively higher inhibitory activity against the tested bacterial strains compared to dsDNA/CuNCs. These results indicated that DNS/CuNCs possessed greater antibacterial activity than dsDNA/CuNCs. Subsequently, we used the plate counting method to further evaluate the antibacterial activity of dsDNA/CuNCs and DNS/CuNCs. As shown in Fig. 2A and B, compared with the PBS group, treatment with dsDNA/CuNCs had little effect on the number of bacterial colonies, whereas treatment with DNS/CuNCs resulted in a reduction in the number of colonies. When compared to the H_2O_2 group, the colony count in the DNS/CuNCs + H_2O_2 treatment was markedly lower, with only a few scattered colonies remaining. These finding indicated that DNS/CuNCs influence bacterial activity. Furthermore, the reduction in colony numbers in the DNS/CuNCs + H_2O_2 group was even more pronounced than in the DNS/CuNCs group, suggesting that the antibacterial effect of the combination of DNS/CuNCs and H_2O_2 is significantly

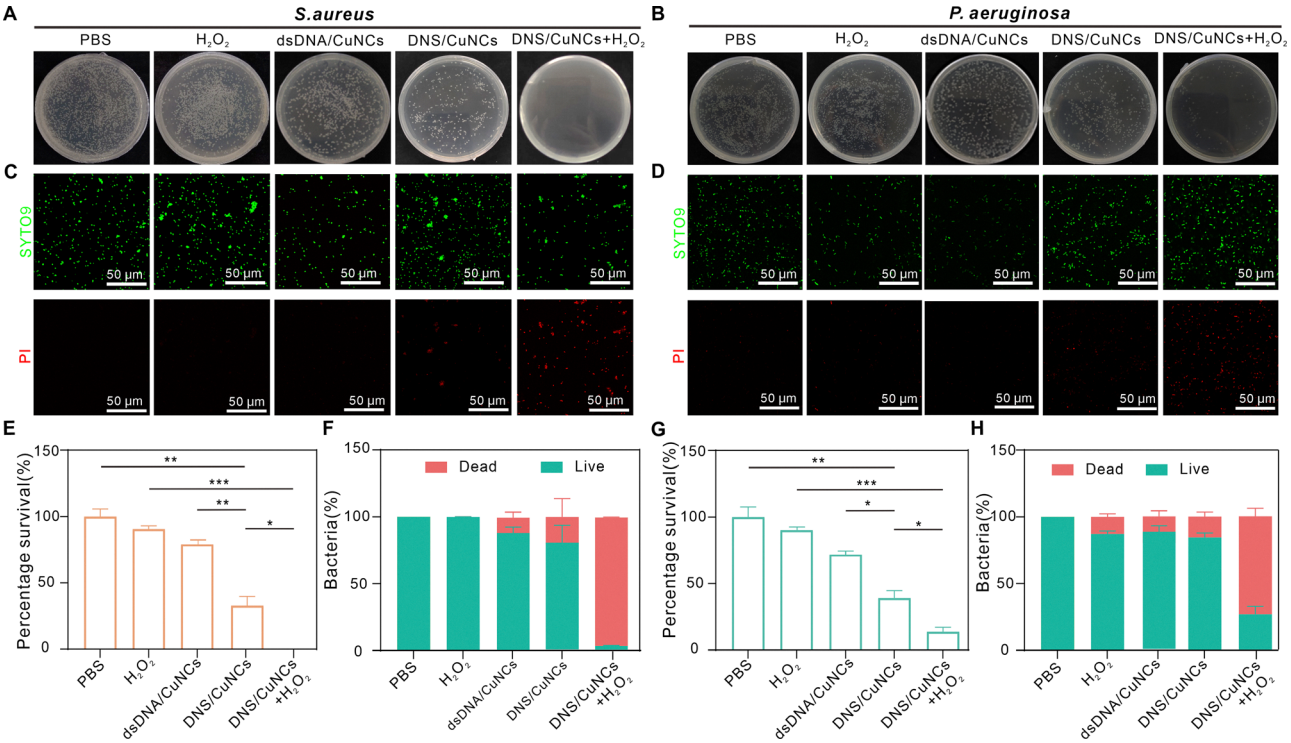

Fig. 2 Bacterial colony images of *S. aureus* (A) and *P. aeruginosa* (B) treated with PBS, H_2O_2, dsDNA/CuNCs, DNS/CuNCs, and DNS/CuNCs + H_2O_2. Percentage survival of *S. aureus* (E) and *P. aeruginosa* (G) after treatment according to (A) and (B). Fluorescence staining images of *S. aureus* (C) and *P. aeruginosa* (D) using SYTO9/PI after different treatments. Bacterial live and dead rates of *S. aureus* (F) and *P. aeruginosa* (H) after (C) and (D) treatment. The asterisks are used to indicate significant difference; n.s. indicates no significant difference.

stronger than that of either component used independently. To further quantify these observations, colony-forming units (CFUs) were counted to assess the toxicity of DNS/CuNCs towards the bacteria. The quantitative analysis is presented in Fig. 2E and G. Compared to the PBS group, the survival rate of bacterial cells in the DNS/CuNCs group significantly decreased, exhibiting an inhibition rate of 67.42% against *S. aureus* and 60.91% against *P. aeruginosa*. The inhibition rates of the dsDNA/CuNCs group against the two bacterial strains were both lower than 27.3%, which was significantly lower than the inhibitory effect of the DNS/CuNCs group. In contrast to H_2O_2, the inhibition rate in the DNS/CuNCs + H_2O_2 group increased dramatically, surpassing 99.96% against *S. aureus* and 86.35% against *P. aeruginosa*, demonstrating a markedly greater inhibitory effect than that observed in the DNS/CuNCs group. Additionally, the antibacterial effect of DNS/CuNCs was visualized using live/dead double-staining fluorescent dyes (SYTO9/propidium iodide, PI) (Fig. 2C and D). After co-culturing the bacterial suspension with DNS/CuNCs, the DNS/CuNCs were removed prior to staining to prevent SYTO9 from staining the DNS/CuNCs, which could otherwise interfere with the experimental outcomes. The SYTO9 could stain all bacterial cells with green fluorescence, while PI stained only cells with compromised membranes with red fluorescence. When both SYTO9 and PI stained the same cells, the red fluorescence of PI was noticeably enhanced, indicating compromised membrane integrity. As seen in Fig. 2C and D, untreated *S. aureus* and *P. aeruginosa* (PBS group) showed solely bright green fluorescence, with no red fluorescence, indicating intact cell walls and membranes. Compared to the PBS group, the dsDNA/CuNCs treatment exhibited negligible red fluorescence, whereas the DNS/CuNCs treatment produced weak red fluorescence. In contrast to the H_2O_2 group, the treatment with DNS/CuNCs + H_2O_2 generated strong red fluorescence, which was more intense than that of DNS/CuNCs alone. The intensity of the red fluorescence was more pronounced in *S. aureus* than in *P. aeruginosa*, indicating a stronger antibacterial effect against Gram-positive bacteria. Quantitative analysis further revealed that the survival rate of *S. aureus* and *P. aeruginosa* in the DNS/CuNCs treatment group was approximately 80% compared to the PBS group, while the survival rate in the dsDNA/CuNCs treatment group was over 90% (Fig. 2F and H). In contrast to the H_2O_2 treatment group, the survival rates of *S. aureus* and *P. aeruginosa* treated with DNS/CuNCs + H_2O_2 were reduced to 2.8% and 26.4%, respectively, demonstrating greater efficacy than the DNS/CuNCs treatment group. These results consistently indicated that dsDNA/CuNCs exhibited almost no antibacterial activity, while DNS/CuNCs exhibited limited antibacterial performance. Notably, the antibacterial performance of DNS/CuNCs was significantly enhanced when combined with H_2O_2, particularly against Gram-positive bacteria such as *S. aureus*. This may be due to the structural differences between Gram-negative and Gram-positive bacteria, as the outer membrane of Gram-negative bacteria—composed of glycerophospholipids,

lipopolysaccharides, and lipoproteins—provided additional protection against antibacterial agents, allowing these bacteria to better adapt to external environments.[18] To further verify the role of DNS/CuNCs, we investigated the antibacterial properties of CuNPs + H_2O_2 and dsDNA/CuNCs + H_2O_2. As shown in Fig. S9, both CuNPs + H_2O_2 and dsDNA/CuNCs + H_2O_2 exhibited very weak antibacterial activity, far lower than that of DNS/CuNCs + H_2O_2. These results indicated that the ultrathin nanosheets of DNS/CuNCs offer superior antibacterial performance compared to smaller-sized spherical structures, further confirming the inherent antibacterial effects of the DNS/CuNCs material. Then, we investigated the copper ion release of DNS/CuNCs using ICP-MS (Fig. S10). The copper ion concentration fell by 19.18 ng mL^{-1} in 12 h, 7.9 ng mL^{-1} at 12–48 h, 9.8 ng mL^{-1} at 48–72 h, and 11.2 ng mL^{-1} at 72–120 h. These data suggested that copper ions were slowly released from DNS/CuNCs into the surrounding area to exert their effects.

Inhibition of biofilm formation

DNS/CuNCs exhibit certain advantages in antibacterial activity and hold promise as an effective measure for treating infections. However, the formation of biofilms significantly increases the difficulty of treating infections. Therefore, it is necessary to further investigate the impact of DNS/CuNCs on biofilms. Our initial focus investigated the ability of DNS/CuNCs to inhibit biofilm formation prior to its establishment. Gram-negative (*P. aeruginosa*) bacteria were selected as the bacterial model. The ability of DNS/CuNCs to inhibit surface biofilm formation was evaluated using crystal violet staining and calcein AM staining, observed using confocal laser scanning microscopy (CLSM). Both CLSM and crystal violet staining revealed substantial biofilm aggregation in the PBS and DNS groups, whereas treatment with DNS/CuNCs significantly reduced both the thickness and amount of biofilm (Fig. 3A and B). Co-incubation with DNS/CuNCs markedly suppressed *P. aeruginosa* biofilm growth, resulting in an 87% reduction in biofilm biomass compared to the PBS group (Fig. 3B). These results demonstrated that DNS had negligible effects on inhibiting biofilm formation, whereas DNS/CuNCs effectively inhibited biofilm development and hold promise as an effective strategy for controlling infections caused by bacterial biofilms.

The initial surface attachment during biofilm formation facilitates bacterial migration, as bacteria seek optimal nutritional conditions through mechanisms such as twitching and swarming motility.[19] These social behaviors share overlapping genetic regulation and play a crucial role in biofilm development and maintenance.[20] *P. aeruginosa* is particularly well-studied in this context, and the twitching motility driven by type IV pili in a "grappling hook" motion, facilitates rapid surface colonization and contributes to both early biofilm formation and the dispersion of mature biofilms.[21] The influence of DNS/CuNCs on *P. aeruginosa* twitching motility was examined, and a notable reduction of 57.5% was observed compared to the PBS group (Fig. 3C and D). Swarming motility involves the coordinated, rapid movement of bacterial groups across a semisolid surface.[22] As shown in Fig. 3E, treatment with DNS/CuNCs significantly reduced the swarming ability of

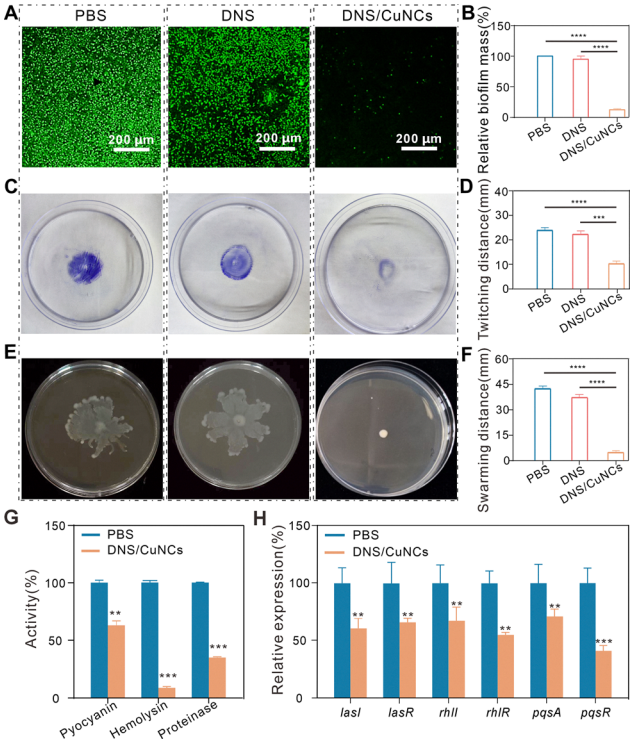

Fig. 3 (A) Confocal fluorescence staining of *P. aeruginosa* biofilms attachment under different treatments. (B) Relative biofilm mass of biofilm stained with crystal violet of *P. aeruginosa* after different treatments. (C) Phenomenon and (D) statistical chart of different treatments on the twitching motility of *P. aeruginosa*. (E) Phenomenon and (F) statistical chart of different treatments on the Swarming motility of *P. aeruginosa*. (G) Effect of DNS/CuNCs on the secretion of virulence factors of *P. aeruginosa*. (H) Measurement of transcription levels of QS regulated genes under DNS/CuNCs treatment using qRT PCR. The asterisks are used to indicate significant difference; n.s. indicates no significant difference.

P. aeruginosa, resulting in an 89.7% decrease in the swarming diameter (Fig. 3F). In contrast, the DNS group resulted in a reduction of only 5.2% and 8.1% in the diameters of twitching and swarming motility, respectively. These findings indicated that DNS have negligible effects on bacterial motility, whereas the inhibitory effects of DNS/CuNCs on bacterial motility further contribute to the suppression of biofilm formation. The impact of DNS/CuNCs on biofilms was also assessed by measuring levels of virulence factor secretion. Compared to the PBS group, treatment with DNS/CuNCs inhibited pyocyanin production by 37.1%, protease production by 64.6%, and hemolysin production by 91.2% (Fig. 3G). This significant decrease correlated with the previously mentioned experimental results, suggesting that the reduction in virulence factor secretion by DNS/CuNCs may also have played a role in inhibiting bacterial biofilms.

Bacterial motility and virulence factor secretion are regulated by the quorum sensing (QS) system, which involves population-dependent signaling to control gene expression and coordinate biofilm growth and virulence factor production.[23] To assess the impact of DNS/CuNCs on the QS system, qRT-PCR was used to measure the transcription levels of QS-regulated genes. The expression of four LasR-activated genes—lasI, lasR, rhlI, and rhlA—was

downregulated by DNS/CuNCs by 40%, 34%, 33%, and 45%, respectively (Fig. 3H). Additionally, the expression levels of pqsA and pqsR, which are critical components of the 2-heptyl-3-hydroxy-4-quinolone (PQS) signaling pathway involved in the synthesis of PQS,[23] were reduced by 30% and 59%, respectively (Fig. 3H). These results indicated that DNS/CuNCs may inhibit quorum sensing regulation, potentially through the suppression of LasR and PqsR activity. Collectively, these results demonstrated that DNS/CuNCs could inhibit the expression of key QS regulatory factors (particularly LasR and PqsR), thereby affecting bacterial motility and the secretion of virulence factors, ultimately suppressing the formation of bacterial biofilms. In conclusion, DNS/CuNCs show significant potential in preventing infections caused by biofilm formation.

Anti-biofilm of DNS/CuNCs *in vitro*

The formation of biofilms significantly increases the difficulty of treating infections, making the removal of established surface biofilms a challenging task. Therefore, we further investigated the ability of DNS/CuNCs to eradicate preformed biofilms. *P. aeruginosa*, a notorious biofilm-forming pathogen, is highly adept at forming dense biofilms within 24 hours under laboratory conditions. The ability of *P. aeruginosa* to form biofilms is a key factor contributing to its persistence in human infections.[24] Mature *P. aeruginosa* biofilms were cultivated using confocal dishes and then treated with different material groups. Subsequently, the biofilms were stained with Calcein AM and visualized using confocal microscopy. As shown in Fig. 4A, compared with the PBS group, the biofilm treated with dsDNA/CuNCs exhibited no significant changes, whereas the biofilm treated with DNS/CuNCs showed a certain degree of disruption, albeit with limited efficacy. However, compared to the H_2O_2 group, the fluorescence intensity of the DNS/CuNCs + H_2O_2 group decreased sharply, indicating that a large amount of biofilm was detached from the surface of the

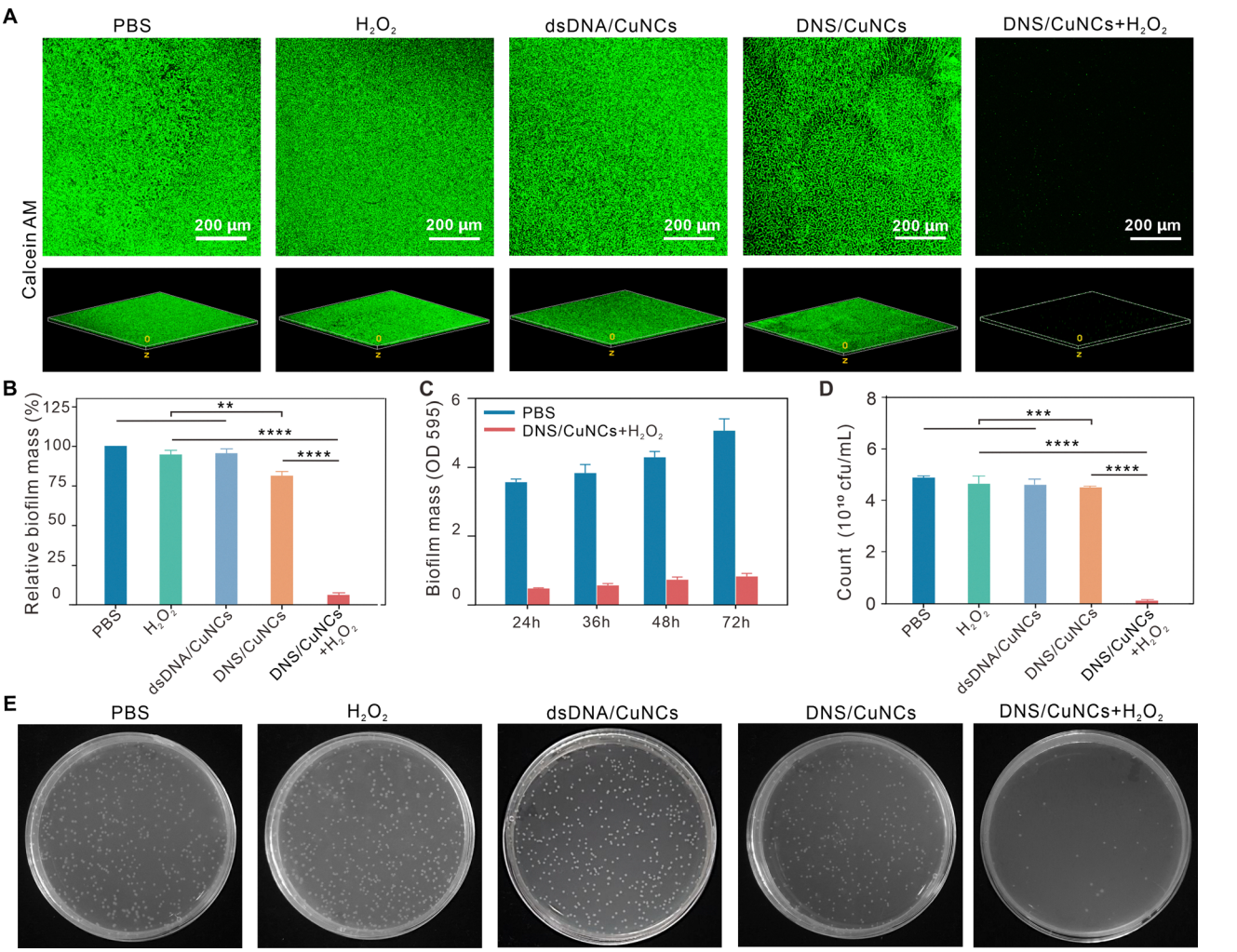

Fig. 4 (A) Confocal microscopy fluorescence staining images of *P. aeruginosa* biofilms treated with PBS, H_2O_2, dsDNA/CuNCs, DNS/CuNCs, and DNS/CuNCs + H_2O_2. (B) Relative biomass mass of residual *P. aeruginosa* biofilm after different treatments. (C) Biofilm mass after DNS/CuNCs + H_2O_2 treatment at different incubation times (24 h, 36 h, 48 h, 72 h). (D) Statistical charts of colony morphology of *P. aeruginosa* on agar plates after different treatments. (E) Colony morphology of *P. aeruginosa* on agar plates after different treatments. The asterisks are used to indicate significant difference; n.s. indicates no significant difference.

culture medium after treatment, leading to the destruction of mature biofilm—this effect was much stronger than that of the DNS/CuNCs treatment. To quantify the effect of DNS/CuNCs + H_2O_2 on the total biofilm biomass, crystal violet staining was subsequently employed. As shown in Fig. 4B, compared to the PBS group, the DNS/CuNCs treatment only reduced the biomass by 16.69%. In contrast, the DNS/CuNCs + H_2O_2 treatment group resulted in a 93.90% reduction in biofilm biomass compared to the H_2O_2 group, which was significantly higher than that of DNS/CuNCs. The results indicated that dsDNA/CuNCs had no effect on biofilms, DNS/CuNCs exerted minimal influence on biofilms, whereas the combination of DNS/CuNCs and H_2O_2 could effectively disrupt biofilms. We further examined the disruption efficacy of DNS/CuNCs + H_2O_2 on biofilms formed over different lengths of incubation (*e.g.*, 24 h, 36 h, 48 h, and 72 h). As shown in Fig. 4C, compared to the PBS group, significant biomass reductions were observed across all incubation times following treatment with DNS/CuNCs + H_2O_2. Following the anti-biofilm assay, the residual biofilm was sonicated, and the dispersions were cultured on LB agar plates. As shown in Fig. 4E, compared with the PBS group, dsDNA/CuNCs had almost no effect, while the effect of DNS/CuNCs was relatively small. In contrast to H_2O_2 alone, the combination of DNS/CuNCs + H_2O_2 effectively disrupted bacterial colonies within mature *P. aeruginosa* biofilms, leading to a sharp decrease in bacterial density. Quantitative analysis using colony-forming units (CFUs) on agar plates (Fig. 4D) indicated that, compared with the PBS group, treatment with DNS/CuNCs reduced the number of bacterial colonies in mature biofilms by 1.75×10^7 cfu mL^{-1}. Compared with the H_2O_2 treatment group, treatment with DNS/CuNCs + H_2O_2 reduced the number of bacterial colonies in mature biofilms 4.7×10^7 cfu mL^{-1}. These findings confirmed that the ability of DNS/CuNCs + H_2O_2 to kill bacteria within biofilms was significantly superior to that of DNS/CuNCs alone, consistent with the *in vitro* antibacterial results. These favorable outcomes demonstrated that while DNS/CuNCs alone had minimal impact on biofilms, the combination of DNS/CuNCs + H_2O_2 could significantly enhance the ability to disrupt biofilms.

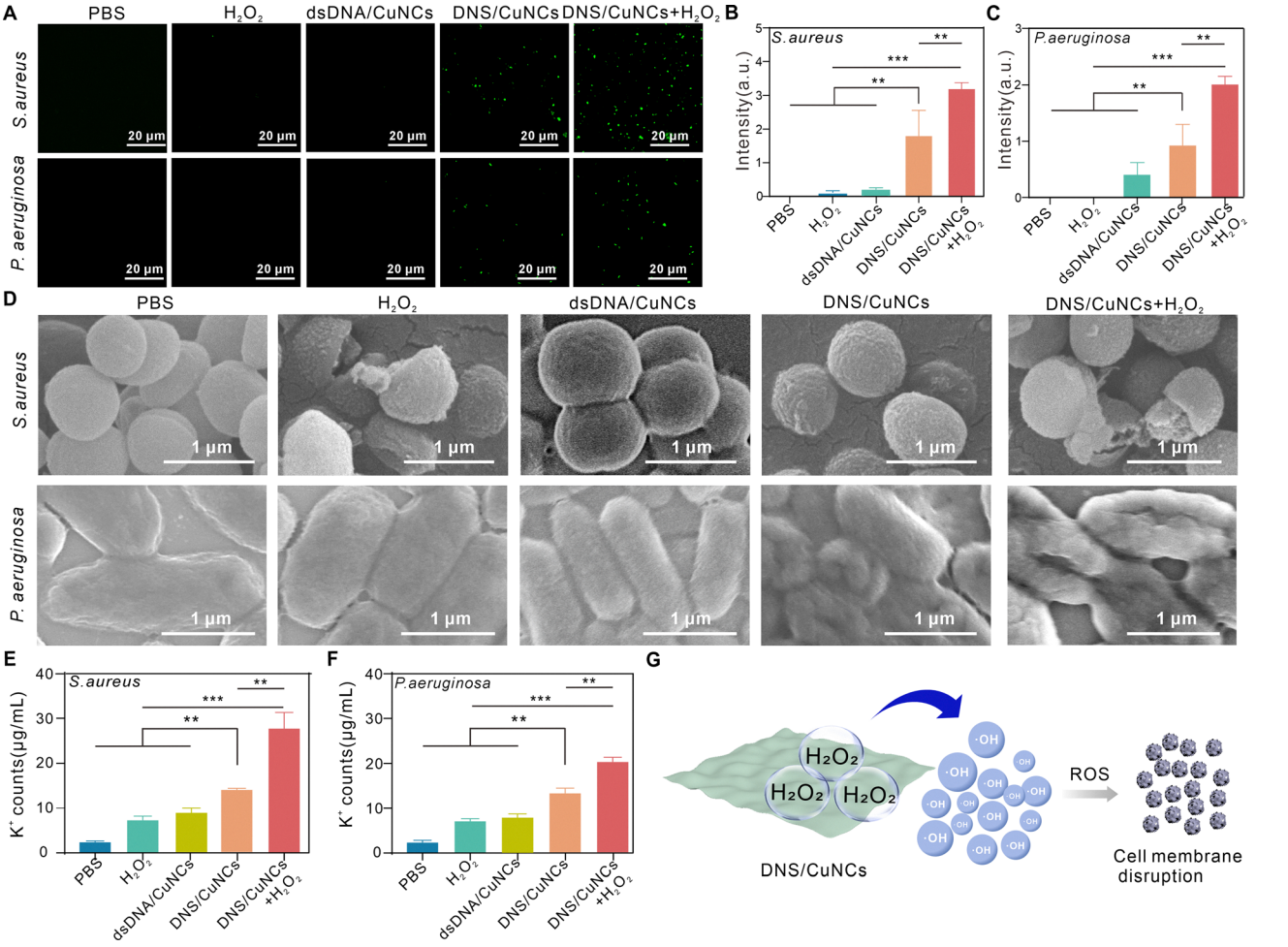

Fig. 5 (A) ROS confocal fluorescence staining of *S. aureus* and *P. aeruginosa* after different treatments. ROS fluorescence intensity statistics of *S. aureus* (B) and *P. aeruginosa* (C) after different treatments. (D) SEM analysis of *S. aureus* and *P. aeruginosa* after different treatments. The release of K^+ from *S. aureus* (E) and *P. aeruginosa* (F) with treated different treatments. (G) Schematic diagram of ROS–•OH generation by DNS/CuNCs under the joint action of H_2O_2. The asterisks are used to indicate significant difference; n.s. indicates no significant difference.

Mechanism of DNS/CuNCs in treating infections

In the preceding section, we found that DNS/CuNCs combined with H_2O_2 exhibited significantly enhanced antibacterial properties and biofilm-disrupting capabilities. However, DNS/CuNCs alone also possessed a limited degree of antibacterial and biofilm-disrupting abilities. The antibacterial and antibiofilm mechanisms of DNS/CuNCs were investigated by detecting the levels of intracellular ROS in bacteria, which are closely related to bacterial cell death, and biofilm disruption. The 2′,7′-dichlorodihydrofluorescein diacetate (DCFH-DA) assay was employed to assess the levels of intracellular ROS in bacteria. In this assay, bacterial cellular esterases deacetylate DCFH-DA, which is subsequently oxidized by ROS to form the green fluorescent compound 2′,7′-dichlorofluorescein (DCF). Changes in the ROS levels in *S. aureus* and *P. aeruginosa* under DNS/CuNCs treatment conditions were examined. Experimental data revealed that the fluorescence intensity of *S. aureus* treated with DNS/CuNCs was 1.8 times higher than that of the PBS group (Fig. 5A and B), and the fluorescence intensity of *P. aeruginosa* treated with DNS/CuNCs was 0.9 times higher than that of the PBS group (Fig. 5A and C). The fluorescence intensity of bacteria treated with dsDNA/CuNCs was all below 0.4%. These findings suggested that DNS/CuNCs elevated the intracellular ROS levels in bacteria. These results were consistent with the intracellular fluorescence observed in mature *P. aeruginosa* biofilms treated with DNS/CuNCs (Fig. S11). To intuitively observe the effects of DNS/CuNCs on bacteria, we employed scanning electron microscopy (SEM) to analyze the morphological changes induced by DNS/CuNCs on *S. aureus* and *P. aeruginosa*. As shown in Fig. 5D, the SEM images of the PBS and dsDNA/CuNCs groups revealed intact bacteria with smooth surfaces. In contrast, treatment with DNS/CuNCs alone resulted in both *S. aureus* and *P. aeruginosa* exhibiting slight wrinkling and rupture, indicating that DNS/CuNCs compromised the integrity of bacterial cell membranes. Since the rupture of the cell membrane could lead to the leakage of intracellular substances, we measured the changes in extracellular K^+ concentration in bacteria after DNS/CuNCs treatment using inductively coupled plasma mass spectrometry (ICP-MS). Compared to PBS, treatment with DNS/CuNCs resulted in 5.7 times increase in extracellular K^+ concentration in *S. aureus* (Fig. 5E) and 5.5 times increase in extracellular K^+ concentration in *P. aeruginosa* (Fig. 5F). The changes in extracellular K^+ concentration of bacteria treated with dsDNA/CuNCs were all below 10%. These changes suggested that the leakage of intracellular K^+ may be attributed to the rupture of the bacterial cell membrane. Based on these observations, we speculated that the antibacterial and antibiofilm mechanisms of DNS/CuNCs may involve limited damage to bacteria and biofilms through the physical cutting action of DNS/CuNCs, leading to the leakage of intracellular K^+ and a moderate increase in intracellular ROS levels. According to literature reports, ultrathin nanosheets can achieve antibacterial effects through physical disruption. Chen *et al.*[25] found that Janus MoSSe nanosheets can effectively insert into bacterial membranes, thereby disrupting the normal structure of the bacterial membrane and exhibiting significant antibacterial activity. Liu *et al.*[26] discovered that the lateral size of graphene oxide (GO) was a key factor affecting its antibacterial activity, with larger lateral size graphene oxide nanosheets demonstrating higher antibacterial efficiency. The dsDNA/CuNCs possessed similar fundamental material properties to DNS/CuNCs but lacked the unique ultrathin structure and large lateral dimensions of DNS/CuNCs. Therefore, the impact of dsDNA/CuNCs on bacterial cells and biofilms could be considered negligible. This observation highlighted the essential role of the ultrathin structure and large lateral dimensions in DNS/CuNCs, which are essential for their distinctive antibacterial and biofilm-disrupting activities. Consequently, the absence of these dimensions in dsDNA/CuNCs explained their inability to replicate the effects observed with DNS/CuNCs. Collectively, these results substantiated the significant contribution of the physical cutting effect, attributed to the unique structural characteristics of DNS/CuNCs, to their mechanisms of antibacterial action and biofilm disruption.

Based on our previous studies, DNS/CuNCs possess peroxidase-like activity, which can catalyze H_2O_2 to generate a large amount of ROS,[27] theoretically inducing bacterial death and biofilm disruption. To evaluate the peroxidase-like catalytic activity of DNS/CuNCs, 3,3′,5,5′-tetramethylbenzidine (TMB) was used as a substrate. After being oxidized by hydrogen peroxide (H_2O_2), TMB changed color from colorless to blue. In experiments, neither the DNS/CuNCs + TMB group nor the DNS/CuNCs + H_2O_2 group produced a color change or an absorption peak at 652 nm. However, the DNS/CuNCs + TMB + H_2O_2 group exhibited the strongest absorption peak at 652 nm (Fig. S12) and a color change of turning blue, demonstrating the peroxidase-like catalytic activity in DNS/CuNCs. To further clarify the catalytic mechanism, electron paramagnetic resonance (EPR) was performed to identify the radicals present in the reaction system. The spectrum in Fig. S13 revealed a characteristic signal with a 1 : 2 : 2 : 1 intensity ratio, confirming the generation of $^{\bullet}OH$ radicals during the catalytic process. To further confirm the peroxidase-like activity of DNS/CuNCs, we analyzed their enzyme activity kinetics, obtaining a K_m value of 0.744 mM and a V_{max} of 14.25×10^{-8} M s^{-1} (Fig. S14 and Table S2). The enzyme-catalyzed reaction rate of DNS/CuNCs demonstrated here surpasses that of several previously reported nanozymes (Table S2). Given that infected bacterial wounds develop an acidic environment due to the inflammatory response and localized hypoxia, the enzymatic activity of DNS/CuNCs in such conditions was critical. The peroxidase-like activity of DNS/CuNCs across different pH levels was therefore verified. Fig. S15 showed that the peroxidase-like activity increased as pH decreased, which aligns with the mildly acidic conditions of infected wounds and may enhance their therapeutic effectiveness in treating wound infections.

Given the peroxidase-like activity of DNS/CuNCs, we investigated the intracellular ROS levels in bacteria and biofilms treated with DNS/CuNCs + H_2O_2. As shown in Fig. 5A and B, the fluorescence intensity of *S. aureus* treated with DNS/CuNCs + H_2O_2 was 3 times higher than that of the H_2O_2 group and 1.2 times higher than that of the DNS/CuNCs group. For *P. aeruginosa*, the fluorescence intensity of the DNS/CuNCs + H_2O_2

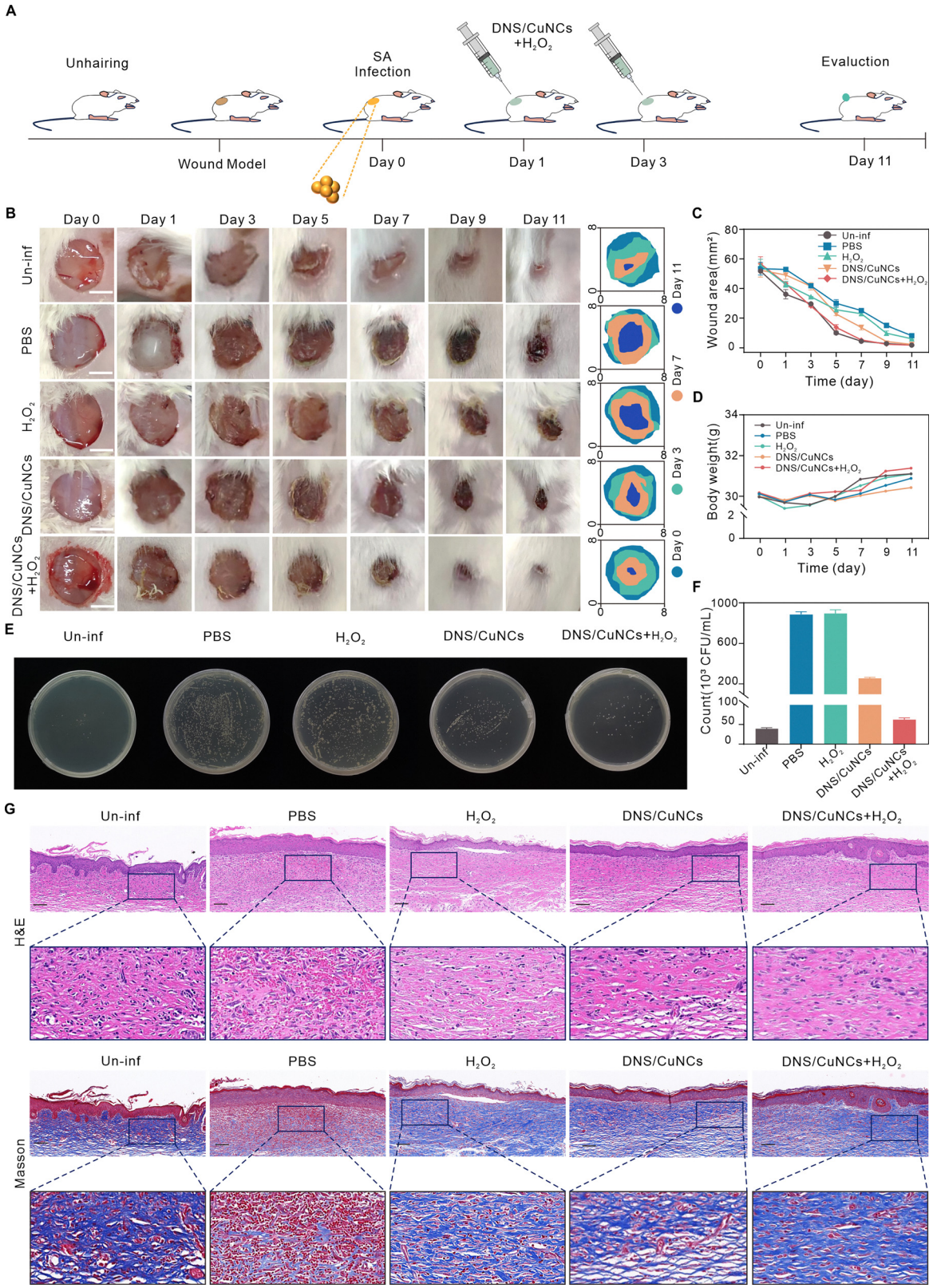

Fig. 6 (A) Schematic diagram of wound infection of *S. aureus* in mice treated with DNS/CuNCs + H_2O_2. (B) Wound diagram and (C) wound area of DNS/CuNCs + H_2O_2 and other experimental groups of mice. (D) Body weight of mice in different experimental groups on days 1–11. (E) Wound plates and (F) statistical graphs of mice in different experimental groups. (G) Histopathology images of the wound skin in different experimental groups of mice after 11 days.

treatment group was two times higher than that of the H_2O_2 group and 1.1 times higher than that of the DNS/CuNCs group (Fig. 5A and C). Concurrently, the production of ROS was further verified through fluorescence spectroscopy. Fig. S16 demonstrated that the fluorescence intensity of DNS/CuNCs + H_2O_2 was the highest. These findings indicated that DNS/CuNCs + H_2O_2 led to a significant increase in ROS levels within the bacteria, surpassing the increase caused by DNS/CuNCs alone. The ROS levels in mature *P. aeruginosa* biofilms treated with DNS/CuNCs + H_2O_2 exhibited similar results (Fig. S11). To further study the morphology of bacteria, SEM observations were conducted, as shown in Fig. 5D. In comparison to the H_2O_2 group, bacteria treated with DNS/CuNCs + H_2O_2 exhibited significant shrinkage and rupture, with the degree of damage being markedly greater than that observed with DNS/CuNCs treatment alone. As expected, compared with treatment with H_2O_2 alone, treatment with DNS/CuNCs + H_2O_2 resulted in 3.8 times increase in the extracellular K^+ concentration in *S. aureus* (Fig. 5E) and 2.8 times increase in *P. aeruginosa* (Fig. 5F). When compared to DNS/CuNCs treatment, the extracellular K^+ concentration of *S. aureus* increased by 2 times (Fig. 5E) and that of *P. aeruginosa* increased by 1.5 times (Fig. 5F) after treatment with DNS/CuNCs + H_2O_2. These findings indicated that treatment with DNS/CuNCs + H_2O_2 resulted in cell membrane rupture, leading to intracellular K^+ leakage, with the extent of leakage being significantly greater than that observed with DNS/CuNCs treatment alone. The effects produced by the DNS/CuNCs + H_2O_2 treatment may be attributed to the peroxidase activity of DNS/CuNCs, which catalyzes H_2O_2 into hydroxyl radicals ($^{\bullet}OH$), thereby damaging bacterial cell membranes and biofilms, resulting in increased intracellular ROS levels (Fig. 5G) and intracellular K^+ leakage. However, although DNS/CuNCs exhibited lower antibacterial and biofilm-disrupting capabilities compared to DNS/CuNC + H_2O_2, it still possessed some antibacterial and biofilm-disrupting abilities. Therefore, we speculated that the destructive effect of DNS/CuNCs + H_2O_2 on bacteria and biofilms may arise from the synergistic effect of the physical cutting by DNS/CuNCs and their peroxidase activity.

Therapeutic effect of DNS/CuNCs *in vivo*

A murine model of bacterial skin infection is frequently employed to assess the *in vivo* antibacterial efficacy of treatments. Notably, DNS/CuNCs displayed outstanding biosafety for wound healing applications, showing minimal cytotoxicity in mouse epidermal JB6 cells and negligible hemolysis in mouse red blood cells at Cu^{2+} equivalent concentrations as high as 50 μg mL^{-1} (Fig. S17a and b). Since H_2O_2 is the main component of the therapeutic dosage, it is necessary to evaluate the toxic effects of DNS/CuNCs in the presence of H_2O_2. As shown in Fig. S18, DNS/CuNCs exhibited good biocompatibility over 72 hours in the presence of H_2O_2. Given the high bactericidal activity of DNS/CuNCs *in vitro* attributed to their physical cutting and peroxidase-like activity, an *S. aureus*-infected skin wound model was established to further investigate the healing of wounds induced by DNS/CuNCs (Fig. 6A). The results showed that local application of DNS/CuNCs + H_2O_2 effectively suppressed wound infection and significantly accelerated the healing process (Fig. 6B). On the 11th day, the wound area in the PBS-treated group measured 6.45 ± 0.76 mm^2, whereas the areas in the DNS/CuNCs + H_2O_2, DNS/CuNCs, and H_2O_2 treatment groups were 0.05 ± 0.02, 0.57 ± 0.01, and 4.34 ± 0.34 mm^2, respectively (Fig. 6C and Table S3). Treatment with DNS/CuNCs alone showed a degree of therapeutic efficacy, resulted in speeding wound healing and partially alleviating symptoms. This result was reasonable as the physical cutting action of DNS/CuNCs induced a certain degree of rupture in bacterial cell membranes, leading to a moderate increase in intracellular ROS levels, thereby achieving a certain antibacterial effect. However, considering that chronic wounds already have a high resistance to ROS in tissue remodeling, additional ROS may further reduce skin regeneration. According to Fig. 6B, the wound area after treatment with DNS/CuNCs + H_2O_2 was very close to that of uninfected control mice, measuring 0.06 ± 0.03 mm^2, indicating that it could effectively eradicate *S. aureus* and promote the healing of infected wounds. This also suggested that ROS levels were not excessive and did not have a negative impact on the wound healing process. Mice initially exhibited weight loss following *S. aureus* infection, but those treated with DNS/CuNCs + H_2O_2 regained weight more steadily than the PBS group as treatment progressed (Fig. 6D). After treatment, quantitative analysis of bacterial loads in the infected wound sites using the agar plate method revealed a high bacterial count in the PBS and H_2O_2 groups (Fig. 6E). While the DNS/CuNCs treatment showed moderate bacterial inhibition, with a substantial reduction in bacterial numbers observed in the DNS/CuNCs + H_2O_2 group, with *S. aureus* colonies reduced to just 6.97% of those in the PBS group (Fig. 6F). At the conclusion of the treatment period, hematoxylin and eosin (H&E) staining and Masson's staining were performed for histopathological assessment to assess the therapeutic impact of DNS/CuNCs combined with H_2O_2 on infection. (Fig. 6G). Hematoxylin and eosin (H&E) staining of tissue sections from the PBS group showed indistinct cytoplasmic borders and loss of nuclei, indicative of an acute inflammatory response. In contrast, the DNS/CuNCs-treated group displayed partial symptomatic relief. Remarkably, tissue from the DNS/CuNCs + H_2O_2 group showed a return to normal histological morphology. The results of Masson's staining were consistent with those of hematoxylin and eosin (H&E) staining. Therefore, we proposed that DNS/CuNCs + H_2O_2 system was an effective antibacterial treatment for local *S. aureus* infections, capable of accelerating wound healing and mitigating the inflammatory response associated with wound infections.

Conclusions

This work presents DNS/CuNCs as an effective means to antibacterial and anti-biofilm, while exhibiting minimal toxicity to mammalian cells. The results demonstrate that DNS/CuNCs prevent biofilm formation by inhibiting the expression of quorum sensing-related genes, thereby suppressing bacterial

motility and the production of virulence factors. Furthermore, the synergistic effects of the physical ultrathin properties and peroxidase-like activity of DNS/CuNCs result in elevated intracellular ROS levels in bacteria, thereby effectively killing the bacteria and disrupting biofilms. Overall, the introduction of biocompatible DNA-based CuNCs in this study, which combines the material's inherent physical ultrathin properties, peroxidase-like activity and quorum sensing inhibitory gene expression, presents a promising strategy for the prevention and treatment of infections caused by biofilms. This also provides significant potential for advancing biomaterials, developing antibacterial and antibiofilm agents, and preventing biofouling.

Live subject statement

All animal procedures were performed in accordance with the regulations of the Northwest University Animal Management and Welfare Ethics Guidelines and were approved by the Northwest University Animal Management and Ethics Committee (Permit No.: NWU AWC-20220610 M).

Author contributions

The manuscript was written through contributions of all authors. All authors have given approval to the final version of the manuscript. F. C., M. L., J. Luo., and J. L. contributed equally.

Conflicts of interest

The authors declare no competing financial interest.

Data availability

The data supporting this article have been included as part of the SI. The data that support the findings this study are available from the corresponding author upon reasonable request.

Supplementary information available: All experimental methods in the article, additional TEM images, supplementary experimental data, and all DNA sequences used in the experiments. See DOI: **https://doi.org/10.1039/d5nh00257e**

Acknowledgements

This work is supported by the National Natural Science Foundation of China (22422410 and 22374118), the Natural Science Foundation of Shaanxi Province (2022JZ-08 and 2023JC-YB162), the Xi'an Key Laboratory of Functional Supramolecular Structure and Materials (CFZKFKT23004), the Basic Science Research Program for Youths, Shaanxi Institute of Basic Science Research (23JHQ053), and the Open Fund of State Key Laboratory of Chemo/Biosensing and Chemometrics, Hunan University (202162400016).

References

1 M. C. Fitzpatrick, C. T. Bauch and J. P. Townsend, *Nat. Microbiol.*, 2019, **4**, 1612–1619; R. E. Baker, A. S. Mahmud and I. F. Miller, *Nat. Rev. Microbiol.*, 2022, **20**, 193–205; S. K. Ahmed, S. Hussein and K. Qurbani, *J. Med. Surg. Public Health.*, 2024, **2**, 100081; M. Naghavi, S. E. Vollset and K. S. Ikuta, *Lancet*, 2024, **404**, 1199–1226; H. Fongang, A. T. Mbaveng and V. Kuete, *Adv. Bot. Res.*, 2023, **106**, 1–20; K. S. Ikuta, L. R. Swetschinski and G. R. Aguilar, *Lancet*, 2022, **400**, 2221–2248.

2 H. C. Flemming, E. D. van Hullebusch and B. J. Little, *Nat. Rev. Microbiol.*, 2024, 1–19; Z. Liu, K. Guo and L. Yan, *Nat. Commun.*, 2023, **14**, 5132; H. Y. Liu, E. L. Prentice and M. A. Webber, *npj ARR*, 2024, **2**, 27.

3 M. A. Rather, K. Gupta and M. Mandal, *Braz. J. Microbiol.*, 2021, 1–18; S. Sharma, J. Mohler and S. D. Mahajan, *Microorganisms*, 2023, **11**, 1614; R. Mirghani, T. Saba and H. Khaliq, *AIMS Microbiol.*, 2022, **8**, 239.

4 W. Y. Agyeman, A. Bisht and A. Gopinath, *Cureus.*, 2022, **14**, e29956; A. K. Mittal, R. Bhardwaj and P. Mishra, *Open Biotechnol. J.*, 2020, **14**, 107–112; C. L. Ventola, *Pharm. Ther.*, 2015, **40**, 277.

5 S. Suzuki, T. Horinouchi and C. Furusawa, *BMC Genomics.*, 2017, **18**, 1–10; D. G. Larsson and C. F. Flach, *Nat. Rev. Microbiol.*, 2022, **20**, 257–269; T. X. N. Huy, *Beni-Suef Univ. J. Basic*, 2024, **13**, 13.

6 X. Zhu, Q. Tang and X. Zhou, *Pathogenesis*, 2024, **193**, 106741; J. M. V. Makabenta, A. Nabawy and C. Li, *Nat. Rev. Microbiol.*, 2021, **19**, 23–36; G. Muteeb, *Microorganisms*, 2023, **11**, 1489.

7 A. Frei, A. D. Verderosa and A. G. Elliott, *Nat. Rev. Chem.*, 2023, **7**, 202–224; A. Azam, A. S. Ahmed and M. Oves, *Int. J. Nanomed.*, 2012, 6003–6009; Q. Zhang, H. Zhou and P. Jiang, *J. Hazard. Mater.*, 2023, **455**, 131658; S. Stankic, S. Suman and F. Haque, *J. Nano.*, 2016, **14**, 1–20.

8 Y. Pang, Z. Chen and D. Yang, *J. Anal. Test.*, 2023, **7**, 189–203.

9 Q. Xin, H. Shah and A. Nawaz, *Adv. Mater.*, 2019, **31**, 1804838; F. Cui, T. Li and D. Wang, *J. Hazard. Mater.*, 2022, **431**, 128597; S. Huang, Y. Song, J. R. Zhang and X. Chen, *Small.*, 2023, **19**, 2207385; L. Mei, S. Zhu and W. Yin, *Theranostics*, 2020, **10**, 757.

10 V. K. Panthi, K. E. Fairfull-Smith and N. Islam, *Int. J. Pharm.*, 2024, 124046; C. Catuogno and M. N. Jones, *Int. J. Pharm.*, 2003, **257**, 125–140; M. Ferreira, M. Ogren and J. N. R. Dias, *Molecules*, 2021, **26**, 2047.

11 R. Ren, C. Lim and S. Li, *Nanomaterials*, 2022, **12**, 3855; A. G. Niculescu and A. M. Grumezescu, *Mat.*, 2021, **14**, 6812.

12 G. V. Vimbela, S. M. Ngo and C. Fraze, *Int. J. Nanomed.*, 2017, 3941–3965.

13 M. Noga, J. Milan and A. Frydrych, *Int. J. Mol. Sci.*, 2023, **24**, 5133; T. L. Botha, E. E. Elemike and S. Horn, *Sci. Rep.*, 2019, **9**, 4169; G. Vasiliev, A. L. Kubo and H. Vija, *Sci. Rep.*, 2023, **13**, 9202.

14 T. Wu, H. Wang and R. Tian, *Angew. Chem., Int. Ed.*, 2023, **135**, e202311698.

15 Y. Xu, Q. Liu and B. Wang, *Biomater. Sci.*, 2024, **12**, 2331–2340.
16 X. Ouyang, Y. Wu and Y. Gao, *J. Am. Chem. Soc.*, 2023, **145**, 4553–4563.
17 X. Ouyang, Y. Wu and L. Guo, *Angew. Chem., Int. Ed.*, 2023, **62**, e202300893.
18 D. Saxena, R. Maitra and R. Bormon, *NPJ Antimicrob. Resist.*, 2023, **1**, 17; M. Kaur and M. P. Mingeot-Leclercq, *BMC Microbiol.*, 2024, **24**, 186.
19 N. Verstraeten, K. Braeken and B. Debkumari, *Trends Microbiol.*, 2008, **16**, 496–506.
20 D. Kaiser, *Curr. Biol.*, 2007, **17**, 561–570.
21 A. Vishwakarma, F. Dang and A. Ferrell, *J. Am. Chem. Soc.*, 2021, **143**, 9440–9449.
22 D. B. Kearns, *Nat. Rev. Microbiol.*, 2010, **8**, 634–644.
23 Y. Zhang, P. Bhasme and D. S. Reddy, *mLife.*, 2023, **2**, 283–294.
24 A. Haidar, A. Muazzam and A. Nadeem, *Microbe*, 2024, **3**, 100078; F. F. Tuon, L. R. Dantas and P. H. Suss, *Pathogens*, 2022, **11**, 300; F. Kunisch, C. Campobasso and J. Wagemans, *Nat. Commun.*, 2024, **15**, 8572; M. T. T. Thi, D. Wibowo and B. H. Rehm, *Int. J. Mol. Sci.*, 2020, **21**, 8671.
25 J. Chen and Z. Gu, Molecular Landscape of Robust Membrane Disruption by Janus MoSSe Nanosheet, *Colloids Surf., B*, 2025, **254**, 114840.
26 S. Liu, M. Hu and T. H. Zeng, *Langmuir*, 2012, **28**, 12364–12372.
27 L. Li, Y. Ding and M. Lei, *ACS Appl. Mater. Interfaces*, 2024, **16**, 54389–54400.